COMMUNICATIONS IN COMPUTATIONAL PHYSICS
Vol. **2**, No. 5, pp. 1007-1026

Commun. Comput. Phys.
October 2007

Discrete Image Approximations of Ionic Solvent Induced Reaction Field to Charges

Shaozhong Deng* and Wei Cai

Department of Mathematics and Statistics, University of North Carolina at Charlotte, Charlotte, NC 28223-0001, USA.

Received 18 January 2007; Accepted (in revised version) 17 February 2007

Available online 18 April 2007

Abstract. Two methods of discrete images are proposed to approximate the reaction field from ionic solvent for a point charge inside a dielectric spherical cavity. Fast and accurate calculation of such a reaction field is needed in hybrid explicit/implicit solvation models of biomolecules. A first- and a second-order image approximation methods, in the order of $u = \lambda a$ (λ – the inverse Debye screening length of the ionic solvent, a – the radius of the spherical cavity), are derived. Each method involves a point image at the conventional Kelvin image point and a line image along the ray from the Kelvin image point to infinity. Based on these results, discrete point images are obtained by using Jacobi-Gauss quadratures. Numerical results demonstrate that two to three point images are sufficient to achieve a 10^{-3} accuracy in the reaction field with the second-order image approximation.

PACS (2006): 41.20.Cv, 02.60.-x

Key words: Method of images, reaction field, ionic solvent, hybrid solvation model.

1 Introduction

Solvent environment is well-known to provide a crucial contribution to the structure, dynamics and function of biological macromolecules. When modelling biological systems numerically, it has been challenging, however, to account for this environment in a manner that is computationally efficient and physically accurate at the same time. Explicit representation of solvent molecules [1–3] offers a detailed and accurate description of a biological macromolecule, yet the large number of atoms needed limits the size of the simulated system. Alternatively, implicit solvent models [4, 5] reduce the solute-solvent

*Corresponding author. *Email addresses:* shaodeng@uncc.edu (S. Deng), wcai@uncc.edu (W. Cai)

interactions to their mean-field characteristics, expressed as a function of the solute configuration alone, and thus yield significant computational savings. However, these methods also have fundamental limitations due to the fact that the important atomic interaction at the solute-solvent interfaces is ignored. In order to take advantage of the efficiency of the implicit solvent models while also account for structural effects of the solvent in the proximity of the solute, hybrid explicit/implicit solvent models [6–8] have emerged as promising tools for biomolecular simulations. For example, the most common hybrid approach, the solvent shell method [9–12], typically employs explicit solvent only for the first few solvation shells of the solute, with a surrounding dielectric continuum to model bulk effects beyond the shells.

In this paper, we will extend our previous work [13] on discrete image approximations of the reaction field of a dielectric sphere in hybrid solvation models with the pure water solvent to the case of an ionic solvent. Spherical cavities are often used because the reaction field of a spherical dielectric can be solved analytically [12–18]. The main purpose for discrete image approximations to reaction fields is to apply the fast multipole methods directly [13, 19, 20] in calculating the electrostatic interactions among N charges inside the spherical cavity in $\mathcal{O}(N)$ operations.

For the pure water solvent, namely, with no ions present in the solvent, a variety of approaches exist for calculating the reaction field for charges inside the spherical cavity, including Kirkwood's classical series expansion [14], Friedman's image approximation [21], and Abagyan's modified image approximation (MIMEL) [22]. Applications of these image approximations in molecular dynamics or Monte Carlo simulations can be found in [23–27]. All these image approximation methods use only one image charge to represent the reaction field with limited accuracy. Recently, a high-order accurate, multiple image approximation [13] has been proposed based on a theoretical result of over 100 year history dating back to 1883 by C. Neumann [28], which extended the conventional Kelvin image [29] for a conducting sphere to the case of a dielectric one. In the case of a dielectric sphere, an image point charge at the Kelvin image point together with an image line charge along a ray from the Kelvin image point to infinity can be used to represent the reaction field exactly. Lindell and Norris [30–33] have provided the power law distribution for the image line charge density along the ray in 1990s. The high-order accurate, multiple discrete image approximation to the reaction field was then obtained by representing the image line charge with an equivalent set of discrete point charges constructed by using Jacobi-Gauss quadratures [13].

For an ionic solvent, the treatment of charge density due to ions in solution needs special consideration. If we assume that the mobile charge concentrations are given by the Debye-Hückel theory, for a solvent of weak ionic strength the linearized Poisson-Boltzmann equation [34–38] can be used to model the potential field in the solvent. In the case of a spherical cavity, analytical solution of the linearized Poisson-Boltzmann equation goes back to the work published by Kirkwood [14, 17]. Utilizing Kirkwood's basic idea, Alper and Levy proposed a so-called generalized reaction field method for molecular dynamics simulations of liquid water [39]. Although they introduced one or

two ions in the simulation, they did not include ionic strength effects in the reaction field.

In this work, we will construct discrete image approximations for the first time, to the best knowledge of the authors, to the ionic solvent induced reaction field including the effect of ion concentrations. We will first derive a series solution to the ionic solvent induced reaction field by the classical electrostatic theory. Then, following closely the methodology in [30, 33] to approximate the reaction field by a point image at the Kelvin image point and a line image, and the procedures in [13] to further represent the line image by an equivalent set of discrete point images, we will develop first- and second-order discrete image approximations (in terms of the parameter $u=\lambda a$, where λ is the inverse Debye screening length of the ionic solvent, and a is the radius of the spherical cavity) to the ionic solvent induced reaction field. Unlike Alper and Levy's approach, ionic strength effects will be included in the reaction field.

The structure of the paper is as follows. In Section 2, we describe a series solution to the ionic solvent induced reaction field of a point charge inside a dielectric sphere by the classical electrostatic theory. In Section 3, we give a first-order image approximation to the reaction field by a point image at the conventional Kelvin image point and a line image that extends along the radial direction from the Kelvin image point out to infinity. Next, this first-order image approximation is improved by adding a position-independent correction potential, resulting in a second-order image approximation. Section 4 describes the general procedures to discretize the line image by an equivalent set of discrete images. Numerical results are given in Section 5, where accuracy tests are presented to validate the convergence properties of image approximations. Comparisons are made between the method of direct series expansion and the second-order image approximation, and discussions are included on the number of discrete point images needed to achieve certain accuracy. Finally, a conclusion is given in Section 6.

2 Ionic solvent induced reaction field of a point charge

The classical electrostatic theory will be used to find the reaction field due to a point charge inside a dielectric sphere immersed in some ionic solution. The dielectric sphere centering at the origin of coordinates with dielectric constant $\epsilon_{\rm i}$ has radius a, while the point charge q is located on the x-axis inside the sphere at a distance $r_{\rm s}<a$ from the center of the sphere (Fig. 1). The infinite ionic solution, on the other hand, is assumed to be represented as a dielectric continuum of dielectric constant $\epsilon_{\rm o}$.

2.1 Interior potential field

First, the electrostatic potential Φ inside the sphere is given by the Poisson's equation

$$\nabla\cdot(\epsilon_{\rm i}\nabla\Phi(\mathbf{r}))=-4\pi q\delta(|\mathbf{r}-\mathbf{r}_{\rm s}|), \tag{2.1}$$

where $\delta(r)$ is the Dirac delta function. With respect to a spherical coordinate system (r,θ,ϕ) (the pole is denoted by the x-axis in this paper), due to the azimuthal symmetry,

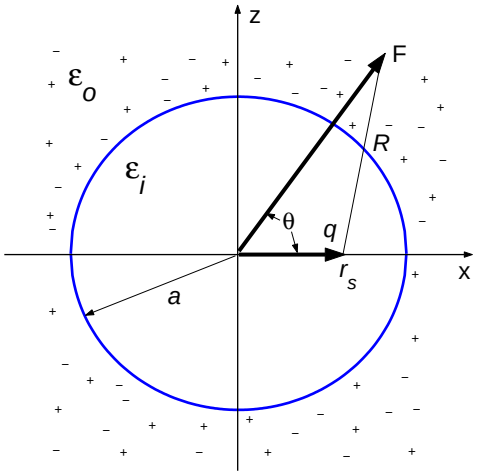

Figure 1: A point charge and a dielectric sphere immersed in an ionic solution.

the potential $\Phi(r,\theta)$ at any field point $\mathbf{r}=(r,\theta,\phi)$ inside the sphere can be expressed in terms of the Legendre polynomials of $\cos\theta$.

More precisely, the potential due to the point charge q alone, the Coulomb potential Φ_{Cou}, is $q/(4\pi\epsilon_{\text{i}}|\mathbf{r}-\mathbf{r}_{\text{s}}|)$. To obtain the total potential field, we need to superimpose on this a reaction field potential Φ_{RF}, due to the polarization of the outside dielectric medium, namely [40],

$$\Phi(r,\theta)=\Phi_{\text{Cou}}(r,\theta)+\Phi_{\text{RF}}(r,\theta)=\frac{q}{4\pi\epsilon_{\text{i}}|\mathbf{r}-\mathbf{r}_{\text{s}}|}+\sum_{n=0}^{\infty}A_n r^n P_n(\cos\theta), \tag{2.2}$$

where $P_n(x)$ and A_n are the Legendre polynomials and the undetermined constant expansion coefficients, respectively.

Meanwhile, the Coulomb potential can also be expanded in terms of the Legendre polynomials of $\cos\theta$ [40]. In particular, the Coulomb potential can be written, when $r_{\text{s}}\leq r\leq a$, as

$$\frac{q}{4\pi\epsilon_{\text{i}}|\mathbf{r}-\mathbf{r}_{\text{s}}|}=\frac{q}{4\pi\epsilon_{\text{i}}r}\sum_{n=0}^{\infty}\left(\frac{r_{\text{s}}}{r}\right)^n P_n(\cos\theta),\qquad r_{\text{s}}\leq r\leq a, \tag{2.3}$$

and when $0\leq r\leq r_{\text{s}}$, as

$$\frac{q}{4\pi\epsilon_{\text{i}}|\mathbf{r}-\mathbf{r}_{\text{s}}|}=\frac{q}{4\pi\epsilon_{\text{i}}r_{\text{s}}}\sum_{n=0}^{\infty}\left(\frac{r}{r_{\text{s}}}\right)^n P_n(\cos\theta),\qquad 0\leq r\leq r_{\text{s}}. \tag{2.4}$$

2.2 Exterior potential field

Let us assume that the mobile ion concentration in the ionic solution is given by the Debye-Hückel theory, i.e., the mobile charges follow a Boltzmann distribution in the

mean field approximation. Then, for the solution of weak ionic strength the linearized Poisson-Boltzmann equation [37, 38]

$$\nabla^2\Phi(\mathbf{r})-\lambda^2\Phi(\mathbf{r})=0 \tag{2.5}$$

can be used to approximate the screened Coulomb potential in the solution. Here, λ is the inverse Debye screening length defined by

$$\lambda^2=\frac{8\pi N_{\rm A}e^2I}{1000\epsilon_{\rm o}k_{\rm B}T},$$

where $N_{\rm A}$ is Avogadro' number, e is the electron charge, $k_{\rm B}$ is the Boltzmann constant, T is the absolute temperature, and I is the ionic strength of the bulk solution. Note that λ^2 is also called the modified Debye-Hückel parameter.

Since the field vanishes at infinity, at any field point $\mathbf{r}=(r,\theta,\phi)$ outside the sphere, the potential $\Phi(\mathbf{r})$ should take the form [40, 41]

$$\Phi(r,\theta,\phi)=\sum_{n=0}^{\infty}\sum_{m=-n}^{n}M_n^m k_n(\lambda r)Y_n^m(\theta,\phi), \tag{2.6}$$

where $Y_n^m(\theta,\phi)$ are the spherical harmonics of degree n and order m, and $k_n(r)$ are the modified spherical Hankel functions of order n (also called the modified spherical Bessel functions of the third kind), respectively. The spherical harmonics can be defined according to the formula

$$Y_n^m(\theta,\phi)=\sqrt{\frac{2n+1}{4\pi}}\sqrt{\frac{(n-|m|)!}{(n+|m|)!}}\,P_n^{|m|}(\cos\theta)e^{{\rm i}m\phi},$$

where $P_n^m(x)$ are the associated Legendre polynomials of degree n and order m, defined by Rodrigues' formula

$$P_n^m(x)=(-1)^m\left(1-x^2\right)^{m/2}\frac{d^m}{dx^m}P_n(x).$$

Furthermore, again due to the axial symmetry of the underlying problem, only terms with $m=0$ remain in Eq. (2.6). By using $P_n^0(x)=P_n(x)$, we obtain the general form for the potential outside the sphere

$$\Phi(r,\theta)=\sum_{n=0}^{\infty}B_n k_n(\lambda r)P_n(\cos\theta), \tag{2.7}$$

where B_n are the undetermined constant expansion coefficients.

The modified spherical Hankel functions are defined in terms of the usual Bessel functions. They can also be explicitly given as [42, 43]

$$k_n(r)=\frac{\pi}{2r}e^{-r}\sum_{k=0}^{n}\frac{(n+k)!}{k!(n-k)!}\frac{1}{(2r)^k},\qquad n=0,1,\cdots. \tag{2.8}$$

For completeness, we include below the two recurrence relations of the modified spherical Hankel functions (for further details, see [42, 43]),

$$\frac{n+1}{r}k_n(r)+\frac{d}{dr}k_n(r)=-k_{n-1}(r), \tag{2.9}$$

$$-\frac{n}{r}k_n(r)+\frac{d}{dr}k_n(r)=-k_{n+1}(r). \tag{2.10}$$

In addition, the asymptotic expression of $k_n(r)$ for $r\to 0$ is

$$k_n(r)\to \pi e^{-r}\frac{(2n)!}{n!}\cdot\frac{1}{(2r)^{n+1}}. \tag{2.11}$$

In summary, the potentials inside and outside the dielectric sphere take the form

$$\Phi(r,\theta)=\begin{cases}\displaystyle\sum_{n=0}^{\infty}\left[\frac{q}{4\pi\epsilon_{\rm i}}\frac{1}{r_{\rm s}}\left(\frac{r}{r_{\rm s}}\right)^n+A_nr^n\right]P_n(\cos\theta), & 0\le r\le r_{\rm s},\\ \displaystyle\sum_{n=0}^{\infty}\left[\frac{q}{4\pi\epsilon_{\rm i}}\frac{1}{r}\left(\frac{r_{\rm s}}{r}\right)^n+A_nr^n\right]P_n(\cos\theta), & r_{\rm s}\le r\le a,\\ \displaystyle\sum_{n=0}^{\infty}B_nk_n(\lambda r)P_n(\cos\theta), & a\le r.\end{cases} \tag{2.12}$$

2.3 Boundary conditions

The expansion coefficients A_n and B_n in (2.12) are to be determined by the boundary conditions that the potentials and the fluxes normal to the spherical boundary are continuous at the boundary, i.e.,

$$\Phi(a^+,\theta)=\Phi(a^-,\theta),\qquad \epsilon_{\rm o}\frac{\partial\Phi(r,\theta)}{\partial r}\bigg|_{r=a^+}=\epsilon_{\rm i}\frac{\partial\Phi(r,\theta)}{\partial r}\bigg|_{r=a^-}.$$

Using the orthogonality of the Legendre polynomials, for all $n\ge 0$ we obtain

$$B_nk_n(\lambda a)=A_na^n+\frac{q}{4\pi\epsilon_{\rm i}}\frac{1}{a}\left(\frac{r_{\rm s}}{a}\right)^n,$$

$$\epsilon_{\rm o}B_n\lambda k_n'(\lambda a)=\epsilon_{\rm i}\left[\frac{q}{4\pi\epsilon_{\rm i}}\frac{-(n+1)}{r_{\rm s}^2}\left(\frac{r_{\rm s}}{a}\right)^{n+2}+nA_na^{n-1}\right].$$

Solving this system for the coefficients A_n and B_n yields, for all $n\ge 0$,

$$A_n=\frac{q}{4\pi\epsilon_{\rm i}a}\frac{1}{r_{\rm i}^n}\frac{\epsilon_{\rm i}(n+1)k_n(u)+\epsilon_{\rm o}uk_n'(u)}{\epsilon_{\rm i}nk_n(u)-\epsilon_{\rm o}uk_n'(u)}, \tag{2.13}$$

$$B_n=\frac{q}{4\pi\epsilon_{\rm i}a}\left(\frac{r_{\rm s}}{a}\right)^n\frac{\epsilon_{\rm i}(2n+1)}{\epsilon_{\rm i}nk_n(u)-\epsilon_{\rm o}uk_n'(u)}, \tag{2.14}$$

where $u=\lambda a$ and $r_{\rm i}=a^2/r_{\rm s}$ with $\mathbf{r}_{\rm i}=(r_{\rm i},0,0)$ denoting the conventional Kelvin image point.

2.4 Zero ionic strength

Before studying the image approximations to the reaction field inside the sphere, let us examine the limit when the ionic strength of the solution, or equivalently the inverse Debye screening length λ, approaches zero. In this case, the arguments of the modified spherical Hankel functions become zero and we can apply their asymptotic expressions for $r\to 0$, i.e., the equation (2.11). Actually, Eq. (2.9) leads to

$$(n+1)k_n(u)+uk_n'(u)=-uk_{n-1}(u), \tag{2.15}$$

and consequently to

$$(n+1)+\frac{uk_n'(u)}{k_n(u)}=-\frac{uk_{n-1}(u)}{k_n(u)},$$

from which and Eq. (2.11), we now obtain

$$\frac{uk_n'(u)}{k_n(u)}\to -(n+1) \qquad \text{as} \quad \lambda\to 0.$$

Note that this implies $uk_n'(u)$ is asymptotically equivalent to $-(n+1)k_n(u)$. Inserting this in Eq. (2.13) yields

$$A_n\to \frac{q}{4\pi\epsilon_i a}\frac{1}{r_i^n}\frac{\epsilon_i(n+1)-\epsilon_o(n+1)}{\epsilon_i n+\epsilon_o(n+1)} \qquad \text{as} \quad \lambda\to 0.$$

On the other hand, it is easy to see from Eq. (2.11) that

$$\frac{k_n(\lambda r)}{k_n(\lambda a)}\to \left(\frac{a}{r}\right)^{n+1} \qquad \text{as} \quad \lambda\to 0.$$

Therefore, we arrive at

$$\begin{aligned} B_n k_n(\lambda r) &= \frac{q}{4\pi\epsilon_i a}\left(\frac{r_s}{a}\right)^n \frac{\epsilon_i(2n+1)}{\epsilon_i n+\epsilon_o(n+1)}\frac{k_n(\lambda r)}{k_n(\lambda a)} \\ &\to \frac{q}{4\pi\epsilon_i r}\frac{\epsilon_i(2n+1)}{\epsilon_i n+\epsilon_o(n+1)}\left(\frac{r_s}{r}\right)^n \qquad \text{as} \quad \lambda\to 0. \end{aligned}$$

These results do not involve the small parameter λ at all, and can be identified with corresponding results for the case of a dielectric sphere immersed in a pure water solution [13].

3 Line image approximations to the reaction field

Let us now turn ourselves to the problem of finding an image outside the spherical region giving rise to the reaction potential inside the sphere. It is well-known that such an image

is not unique, and it could be expressed in the form of a point source like a multipole at any given point, or alternatively a line, surface or volume source. As stated earlier, when no ions exist in the solvent, the problem has been solved independently by C. Neumann, Lindell and Norris [28, 30, 33]. For instance, in the case that a point charge is inside the dielectric sphere, its image can be expressed exactly as a combination of a point image at the classical Kelvin image point and a line image extending along the radial direction from this Kelvin image point out to infinity. For the present problem, however, it is far from clear whether such an exact expression exists or not.

Next, we shall employ an approximating approach to attack this problem. It should be pointed out that, for the proposed approximations to be meaningful, the ionic strength of the solution cannot be too high. In particular, we assume that $u=\lambda a<1$.

3.1 First-order image approximation

To construct the first-order image approximation, we use $e^{-r}=1+\mathcal{O}(r)$ and

$$\sum_{k=0}^{n}\frac{(n+k)!}{k!(n-k)!}\frac{1}{(2r)^k}=\frac{(2n)!}{n!}\frac{1}{(2r)^n}+\mathcal{O}\left(\frac{1}{r^{n-1}}\right).$$

Then the modified spherical Hankel functions (2.8) become

$$k_n(r)=\pi\,\frac{(2n)!}{n!}\frac{1}{(2r)^{n+1}}+\mathcal{O}\left(\frac{1}{r^n}\right),\qquad n\geq 0. \tag{3.1}$$

Consequently, the derivatives of the modified spherical Hankel functions can be expressed as

$$k_n'(r)=-\pi\,\frac{2(n+1)(2n)!}{n!}\frac{1}{(2r)^{n+2}}+\mathcal{O}\left(\frac{1}{r^{n+1}}\right),\qquad n\geq 0. \tag{3.2}$$

Combining Eqs. (3.1) and (3.2) leads to

$$\frac{k_n(r)}{rk_n'(r)}=-\frac{1}{n+1}+\mathcal{O}(r),\qquad n\geq 0. \tag{3.3}$$

Applying this approximation into Eq. (2.13), we now obtain

$$\begin{aligned}A_n&\approx\frac{q}{4\pi\epsilon_{\rm i}a}\frac{1}{r_{\rm i}^n}\frac{\epsilon_{\rm i}(n+1)-\epsilon_{\rm o}(n+1)}{\epsilon_{\rm i}n+\epsilon_{\rm o}(n+1)}\\&=\frac{q}{4\pi\epsilon_{\rm i}a}\frac{1}{r_{\rm i}^n}\left(\gamma+\frac{\delta}{n+\sigma}\right),\qquad n\geq 0,\end{aligned} \tag{3.4}$$

where we denote

$$\gamma=\frac{\epsilon_{\rm i}-\epsilon_{\rm o}}{\epsilon_{\rm i}+\epsilon_{\rm o}},\qquad \sigma=\frac{1-\gamma}{2},\qquad \delta=\frac{\gamma(1+\gamma)}{2}.$$

Note that $-1\leq\gamma\leq 1$ and hence $\sigma\geq 0$. Also, $\gamma=1$ corresponds to the case where the sphere is of infinite dielectric constant ($\epsilon_{\rm i}=\infty$). On the other hand, when $\gamma=-1$ the surrounding solution is of infinite dielectric constant ($\epsilon_{\rm o}=\infty$).

Using (3.4), the reaction field inside the sphere can be approximated as

$$\begin{aligned}\sum_{n=0}^{\infty}A_n r^n P_n(\cos\theta)&\approx\sum_{n=0}^{\infty}\frac{q}{4\pi\epsilon_{\rm i}a}\frac{1}{r_{\rm i}^n}\left(\gamma+\frac{\delta}{n+\sigma}\right)r^n P_n(\cos\theta)\\&=\frac{\gamma q}{4\pi\epsilon_{\rm i}r_{\rm i}}\frac{a}{r_{\rm s}}\sum_{n=0}^{\infty}\left(\frac{r}{r_{\rm i}}\right)^n P_n(\cos\theta)+\frac{\delta q}{4\pi\epsilon_{\rm i}a}\sum_{n=0}^{\infty}\frac{1}{n+\sigma}\left(\frac{r}{r_{\rm i}}\right)^n P_n(\cos\theta)\\&=S_1+S_2.\end{aligned}\tag{3.5}$$

The first series S_1 in (3.5) becomes exactly the expansion given by Eq. (2.3) for a point charge of magnitude $q'=\gamma qa/r_{\rm s}$ outside the sphere at the Kelvin image point $\mathbf{r}_{\rm i}$. For the second series S_2 in (3.5), we need the following integral identity

$$\frac{1}{n+\sigma}=r_{\rm i}^{n+\sigma}\int_{r_{\rm i}}^{\infty}\frac{1}{x^{n+\sigma+1}}{\rm d}x,$$

which is valid for all $n\geq 0$ when $\sigma>0$, namely, when $\epsilon_{\rm i}<\infty$. Inserting this into S_2 leads to

$$\begin{aligned}S_2&=\frac{\delta q}{4\pi\epsilon_{\rm i}a}\sum_{n=0}^{\infty}\left[r_{\rm i}^{n+\sigma}\int_{r_{\rm i}}^{\infty}\frac{1}{x^{n+\sigma+1}}{\rm d}x\right]\left(\frac{r}{r_{\rm i}}\right)^n P_n(\cos\theta)\\&=\int_{r_{\rm i}}^{\infty}\left[\frac{\delta q}{4\pi\epsilon_{\rm i}x}\frac{1}{a}\left(\frac{r_{\rm i}}{x}\right)^{\sigma}\sum_{n=0}^{\infty}\left(\frac{r}{x}\right)^n P_n(\cos\theta)\right]{\rm d}x\\&=\int_{r_{\rm i}}^{\infty}\left[\frac{q''(x)}{4\pi\epsilon_{\rm i}x}\sum_{n=0}^{\infty}\left(\frac{r}{x}\right)^n P_n(\cos\theta)\right]{\rm d}x,\end{aligned}$$

where

$$q''(x)=\frac{\delta q}{a}\left(\frac{x}{r_{\rm i}}\right)^{-\sigma},\qquad r_{\rm i}\leq x.$$

Note that the integrand of the above integral again becomes the expansion given by Eq. (2.3) for a charge of magnitude $q''(x)$ outside the sphere at the point $\mathbf{x}=(x,0,0)$. Therefore, $q''(x)$ can be regarded as a distributed line image charge which stretches from the Kelvin image point $\mathbf{r}_{\rm i}$ along the radial direction out to infinity.

In conclusion, the reaction field inside the sphere due to the charges induced on the surface of the sphere is equal to the field generated by a point image charge q' outside the sphere at the Kelvin image point $\mathbf{r}_{\rm i}$, and a distributed charge that stretches from the Kelvin image point out to infinity with the charge distribution defined by $q''(x)$. This reaction field and the field of the source charge must be added together to find the total field inside the sphere, both the source and the images be taken as acting in a homogeneous material of dielectric constant $\epsilon_{\rm i}$. In other words, the first-order approximation of

the total potential at a field point $\mathbf{r}=(r,\theta,\phi)$ inside the sphere, due to an internal point charge q, consists of three components: the potential $\Phi_s(\mathbf{r})$ from the original source point charge q at $\mathbf{r}_\mathrm{s}$, the potential $\Phi_\mathrm{ip}(\mathbf{r})$ from the image point charge q' at the Kelvin image point $\mathbf{r}_\mathrm{i}$, and the potential $\Phi_\mathrm{il}(\mathbf{r})$ due to the distributed image line charge $q''(x)$, i.e.,

$$\begin{aligned}\Phi(\mathbf{r}) &\approx \Phi_s(\mathbf{r})+\Phi_\mathrm{ip}(\mathbf{r})+\Phi_\mathrm{il}(\mathbf{r})\\ &=\frac{q}{4\pi\epsilon_\mathrm{i}|\mathbf{r}-\mathbf{r}_\mathrm{s}|}+\frac{q'}{4\pi\epsilon_\mathrm{i}|\mathbf{r}-\mathbf{r}_\mathbf{i}|}+\int_{r_i}^{\infty}\frac{q''(x)}{4\pi\epsilon_\mathrm{i}|\mathbf{r}-\mathbf{x}|}\mathrm{d}x.\end{aligned}$$

Remark 3.1. By comparing the approximate expansion coefficients A_n in (3.4) to the corresponding expansion coefficients for the case of a dielectric sphere surrounded by a non-ionic solution, i.e., the coefficients B_n in [13], we find that they are actually identical. This appears to be, but actually is not, surprising since by using the approximation of $k_n(r)$ as described by Eq. (3.1), we are essentially expressing the potential outside the sphere as the same expansion in terms of $P_n(\cos\theta)/r^{n+1}$ as used in [13].

3.2 Second-order image approximation

In essence, the first-order image approximation to the ionic solvent induced reaction field discussed above ignores the ion effect in the reaction field term. In the case that the ionic strength of the solution is not negligible, more accurate image approximations to the reaction field have to be developed.

To derive a second-order image approximation, note that instead of the $\mathcal{O}(1/r^n)$ truncation error as described in Eq. (3.1), we actually have

$$k_n(r)=\pi\,\frac{(2n)!}{n!}\frac{1}{(2r)^{n+1}}+\mathcal{O}\left(\frac{1}{r^{n-1}}\right),\qquad n\geq 1, \tag{3.6}$$

which can be easily verified by expanding $k_n(r)$ in terms of $1/r$. Correspondingly, we have

$$k_n'(r)=-\pi\,\frac{2(n+1)(2n)!}{n!}\frac{1}{(2r)^{n+2}}+\mathcal{O}\left(\frac{1}{r^{n}}\right),\qquad n\geq 1, \tag{3.7}$$

$$\frac{k_n(r)}{rk_n'(r)}=-\frac{1}{n+1}+\mathcal{O}(r^2),\qquad n\geq 1. \tag{3.8}$$

Therefore, we can again conclude

$$A_n\approx\frac{q}{4\pi\epsilon_\mathrm{i}a}\frac{1}{r_\mathrm{i}^n}\left(\gamma+\frac{\delta}{n+\sigma}\right),\qquad n\geq 1. \tag{3.9}$$

For $n=0$, from the exact expression of $k_0(r)$, we arrive at

$$\frac{k_0(r)}{rk_0'(r)}=-\frac{1}{1+r}.$$

Substituting it into A_0 defined in (2.13), we now obtain

$$A_0 = -\frac{q}{4\pi\epsilon_i a}\left(1+\frac{\epsilon_i}{\epsilon_o}\frac{k_0(u)}{uk_0'(u)}\right) = \frac{q}{4\pi\epsilon_i a}\left(\frac{1}{1+u}\frac{\epsilon_i}{\epsilon_o}-1\right). \tag{3.10}$$

Therefore, we have

$$\begin{aligned}\sum_{n=0}^{\infty} A_n r^n P_n(\cos\theta) &\approx A_0 + \sum_{n=1}^{\infty}\frac{q}{4\pi\epsilon_i a}\frac{1}{r_i^n}\left(\gamma+\frac{\delta}{n+\sigma}\right) r^n P_n(\cos\theta)\\ &= \left[A_0 - \frac{q}{4\pi\epsilon_i a}\left(\gamma+\frac{\delta}{\sigma}\right)\right] + \frac{\gamma q}{4\pi\epsilon_i r_i}\frac{a}{r_s}\sum_{n=0}^{\infty}\left(\frac{r}{r_i}\right)^n P_n(\cos\theta)\\ &\quad + \frac{\delta q}{4\pi\epsilon_i a}\sum_{n=0}^{\infty}\frac{1}{n+\sigma}\left(\frac{r}{r_i}\right)^n P_n(\cos\theta)\\ &= S_0 + S_1 + S_2,\end{aligned} \tag{3.11}$$

where S_1 and S_2 in (3.11) are exactly the same as described in the previous subsection. On the other hand, the term S_0 defines a *position-independent* correction potential

$$\Phi_{\text{Cor},1} = \frac{q}{4\pi\epsilon_i a}\left(\frac{1}{1+u}\frac{\epsilon_i}{\epsilon_o}-1-\gamma-\frac{\delta}{\sigma}\right) = -\frac{qu}{4\pi\epsilon_o(1+u)a}. \tag{3.12}$$

Note that $\Phi_{\text{Cor},1}=0$ when $u=\lambda a=0$.

In summary, the second-order approximation of the total potential at a field point $\mathbf{r}=(r,\theta,\phi)$ inside the sphere, due to an internal point charge q, consists of *four* components: the potential $\Phi_s(\mathbf{r})$ from the original source point charge q at $\mathbf{r}_s$, the potential $\Phi_{ip}(\mathbf{r})$ from the image point charge q' at the Kelvin image point $\mathbf{r}_i$, the potential $\Phi_{il}(\mathbf{r})$ due to the distributed image line charge $q''(x)$, and a correction potential $\Phi_{\text{Cor},1}$, i.e.,

$$\begin{aligned}\Phi(\mathbf{r}) &\approx \Phi_s(\mathbf{r}) + \Phi_{ip}(\mathbf{r}) + \Phi_{il}(\mathbf{r}) + \Phi_{\text{Cor},1}\\ &= \frac{q}{4\pi\epsilon_i|\mathbf{r}-\mathbf{r}_s|} + \frac{q'}{4\pi\epsilon_i|\mathbf{r}-\mathbf{r}_i|} + \int_{r_i}^{\infty}\frac{q''(x)}{4\pi\epsilon_i|\mathbf{r}-\mathbf{x}|}\mathrm{d}x + \Phi_{\text{Cor},1}.\end{aligned}$$

Remark 3.2. To further improve the accuracy of the second-order approximation, we can choose to include another *position-dependent* correction potential based on the difference in the dipole moment. More specifically, for $n=1$, using the exact expression of $k_1(r)$, we obtain

$$\frac{k_1(r)}{rk_1'(r)} = -\frac{1+r}{2+2r+r^2}, \tag{3.13}$$

which leads to

$$A_1 = \frac{q}{4\pi\epsilon_i a}\frac{1}{r_i}\frac{2(1+u)\epsilon_i-(2+2u+u^2)\epsilon_o}{(1+u)\epsilon_i+(2+2u+u^2)\epsilon_o}.$$

Then the position-dependent correction potential is defined as

$$\Phi_{\text{Cor},2}(\mathbf{r}) = \frac{q}{4\pi\epsilon_i a}\left[\frac{2(1+u)\epsilon_i-(2+2u+u^2)\epsilon_o}{(1+u)\epsilon_i+(2+2u+u^2)\epsilon_o} - \left(\gamma+\frac{\delta}{1+\sigma}\right)\right]\left(\frac{r}{r_i}\right)\cos\theta.$$

Note that $\Phi_{\text{Cor},2}=0$ when $u=\lambda a=0$. Then, the second-order approximation of the total potential becomes

$$\Phi(\mathbf{r})\approx\frac{q}{4\pi\epsilon_{\text{i}}|\mathbf{r}-\mathbf{r}_{\text{s}}|}+\frac{q'}{4\pi\epsilon_{\text{i}}|\mathbf{r}-\mathbf{r}_{\mathbf{i}}|}+\int_{r_i}^{\infty}\frac{q''(x)}{4\pi\epsilon_{\text{i}}|\mathbf{r}-\mathbf{x}|}\mathrm{d}x+\Phi_{\text{Cor},1}+\Phi_{\text{Cor},2}(\mathbf{r}).$$

As demonstrated in Section 5.1, the inclusion of the position-dependent correction potential greatly improves the accuracy of the second-order image approximation.

4 Discretization of the line image by point images

Now let us show how to construct an equivalent set of image point charges to represent the image line charge introduced in the previous section. The basic idea is to transform the underlying line integral for the potential for an image line charge onto the finite interval $[-1,1]$, and then apply appropriate Gauss or Gauss-Radau quadrature related to specific Jacobi polynomials. Let us begin by approximating the following line integral with an appropriate numerical quadrature

$$I=\int_{r_{\text{i}}}^{\infty}\frac{1}{|\mathbf{r}-\mathbf{x}|}\left(\frac{x}{r_{\text{i}}}\right)^{-\sigma}\mathrm{d}x, \tag{4.1}$$

where $\sigma>0$. First, by introducing the change of variables $r_{\text{i}}/x=((1-s)/2)^{\tau}$ with $\tau>0$, we have

$$I=\tau 2^{-\tau\sigma}\int_{-1}^{1}(1-s)^{\alpha}h(\mathbf{r},s,\tau)\mathrm{d}s, \tag{4.2}$$

where $\alpha=\tau\sigma-1$ and

$$h(\mathbf{r},s,\tau)=\frac{2^{\tau}r_{\text{i}}}{\left|(1-s)^{\tau}\mathbf{r}-2^{\tau}\mathbf{r}_{\mathbf{i}}\right|}. \tag{4.3}$$

Next, we shall employ a numerical quadrature to approximate the integral in Eq. (4.2). Note that $s=-1$ corresponds to the Kelvin image point $x=r_{\text{i}}$. Also $\alpha>-1$ because $\sigma>0$ when $u<1$ and $\tau>0$. Therefore, we can choose either Gauss or Gauss-Radau quadrature based on Jacobi polynomials. The Jacobi polynomials $P_n^{\alpha,\beta}(s)$ on the interval $[-1,1]$ are orthogonal polynomials under the Jacobi weight $w(s)=(1-s)^{\alpha}(1+s)^{\beta}$, i.e.,

$$\int_{-1}^{1}(1-s)^{\alpha}(1+s)^{\beta}P_i^{\alpha,\beta}(s)P_j^{\alpha,\beta}(s)\,\mathrm{d}s=\delta_{ij},$$

where $\alpha>-1$, $\beta>-1$ [44]. More precisely, without losing any generality, let $s_m,\omega_m,m=1,2,\cdots,M$, be the Jacobi-Gauss or Jacobi-Gauss-Radau points and weights on the interval $[-1,1]$ with $\alpha=\tau\sigma-1$ and $\beta=0$ ($s_1=-1$ if Jacobi-Gauss-Radau quadrature is used.) Both s_m and ω_m can be obtained with the program ORTHPOL [44]. Then, the numerical quadrature for approximating the integral in Eq. (4.2) is

$$I\approx\tau 2^{-\tau\sigma}\sum_{m=1}^{M}\omega_m h(\mathbf{r},s_m,\tau). \tag{4.4}$$

Therefore, the potential $\Phi_{\rm il}(\mathbf{r})$ of the line image $q''(x)$ can be approximated by

$$\Phi_{\rm il}(\mathbf{r})=\int_{r_{\rm i}}^{\infty}\frac{q''(x)}{4\pi\epsilon_{\rm i}|\mathbf{r}-\mathbf{x}|}{\rm d}x\approx\sum_{m=1}^{M}\frac{q''_m}{4\pi\epsilon_i|\mathbf{r}-\mathbf{x_m}|}, \tag{4.5}$$

where for $m=1,2,\cdots,M$,

$$q''_m=2^{-\tau\sigma}\tau\delta\omega_m q\,\frac{x_m}{a}, \tag{4.6}$$

and

$$x_m=r_{\rm i}\left(\frac{2}{1-s_m}\right)^{\tau}. \tag{4.7}$$

In conclusion, we have the following image approximations to the total potential inside the sphere in terms of the potentials of $M+2$ point charges.

(a) The first-order approximation:

$$\Phi(\mathbf{r})\approx\frac{1}{4\pi\epsilon_{\rm i}}\left(\frac{q}{|\mathbf{r}-\mathbf{r}_{\rm s}|}+\frac{q'}{|\mathbf{r}-\mathbf{r_i}|}+\sum_{m=1}^{M}\frac{q''_m}{|\mathbf{r}-\mathbf{x_m}|}\right). \tag{4.8}$$

(b) The second-order approximation:

$$\Phi(\mathbf{r})\approx\frac{1}{4\pi\epsilon_{\rm i}}\left(\frac{q}{|\mathbf{r}-\mathbf{r}_{\rm s}|}+\frac{q'}{|\mathbf{r}-\mathbf{r_i}|}+\sum_{m=1}^{M}\frac{q''_m}{|\mathbf{r}-\mathbf{x_m}|}\right)+\Phi_{\rm Cor,1}. \tag{4.9}$$

(c) The second-order approximation with $\Phi_{\rm Cor,2}(\mathbf{r})$:

$$\Phi(\mathbf{r})\approx\frac{1}{4\pi\epsilon_{\rm i}}\left(\frac{q}{|\mathbf{r}-\mathbf{r}_{\rm s}|}+\frac{q'}{|\mathbf{r}-\mathbf{r_i}|}+\sum_{m=1}^{M}\frac{q''_m}{|\mathbf{r}-\mathbf{x_m}|}\right)+\Phi_{\rm Cor,1}+\Phi_{\rm Cor,2}(\mathbf{r}). \tag{4.10}$$

Remark 4.1. Note that $x_1=r_{\rm i}$ when the Jacobi-Gauss-Radau quadrature is employed. Therefore, in this case, after combining together the point image charge q' and the first discrete point charge q''_1, we could have an approximation of the total potential inside the sphere in terms of the potentials of $M+1$ point charges. For instance, for the second-order approximation, we have

$$\Phi(\mathbf{r})\approx\frac{1}{4\pi\epsilon_{\rm i}}\left(\frac{q}{|\mathbf{r}-\mathbf{r}_{\rm s}|}+\frac{q'+q''_1}{|\mathbf{r}-\mathbf{r_i}|}+\sum_{m=2}^{M}\frac{q''_m}{|\mathbf{r}-\mathbf{x_m}|}\right)+\Phi_{\rm Cor,1}. \tag{4.11}$$

Remark 4.2. The parameter $\tau>0$ in the change of variables $r_{\rm i}/x=((1-s)/2)^{\tau}$ can be used as a parameter to control the accuracy of numerical approximations. When $\tau=1/\sigma$ we have $\alpha=0$, and in this case the quadrature given by Eq. (4.4) simply reduces to the Legendre-Gauss or Legendre-Gauss-Radau quadrature. When $\tau=1/(2\sigma)$, we have $\alpha=-1/2$. And when $\tau=3/(2\sigma)$, we have $\alpha=1/2$.

Table 1: Convergence properties of the proposed image approximations.

	First-order		Second-order		Second-order with $\Phi_{\text{Cor},2}$	
$u=\lambda a$	$\|\|E\|\|$	Order	$\|\|E\|\|$	Order	$\|\|E\|\|$	Order
0.8	1.33E-2		3.45E-3		7.27E-4	
0.4	9.54E-3	0.483	1.29E-3	1.418	2.09E-4	1.801
0.2	5.94E-3	0.684	4.02E-4	1.685	5.47E-5	1.931
0.1	3.35E-3	0.824	1.12E-4	1.838	1.39E-5	1.978
0.05	1.79E-3	0.907	2.97E-5	1.918	3.49E-6	1.993
0.025	9.25E-4	0.952	7.65E-6	1.959	8.73E-7	1.998
0.0125	4.70E-4	0.976	1.94E-6	1.979	2.19E-7	1.998

5 Numerical results

For demonstration purpose, let us consider a unit dielectric sphere and a single point charge. We assume that the dielectric constants of the sphere and its surrounding medium are $\epsilon_{\text{i}}=2$ (normally 1, 2 or 4) and $\epsilon_{\text{o}}=80$ (the dielectric constant of water), respectively. We assume further that the single point charge q is located on the x-axis inside the sphere at a distance r_{s} from the center of the sphere. Unless otherwise specified, the Jacobi-Gauss-Radau quadrature is chosen to construct discrete point images, and the parameter τ used in the numerical experiments is chosen as $1/\sigma$. In addition, the results obtained by the series expansion with 400 terms are treated as the exact reaction fields to calculate the errors of various image approximations.

5.1 Accuracy vs the ionic strength

We start by verifying the convergence properties of the proposed image approximations. To this end, in this test the location of the source point charge is fixed at $r_{\text{s}}=0.5$, and the Jacobi-Gauss-Radau quadrature with $M=20$ is employed to approximate the underlying line image. For each selected value of $u=\lambda a$, we calculate the relative error of the image approximations in the reaction field, respectively, at 10,000 observation points uniformly distributed (under the polar coordinates) within the sphere. The maximal relative errors at the 10,000 points for various u values are shown in Table 1, which clearly demonstrates the $\mathcal{O}(\lambda a)$ and $\mathcal{O}((\lambda a)^2)$ convergence properties of the first- and the second-order image approximations, respectively. Moreover, the addition of the position-dependent correction potential $\Phi_{\text{Cor},2}$ to the second-order image approximation can improve its accuracy up to one order higher.

5.2 Accuracy vs the source location

From now on, we shall confine ourselves to the second-order image approximation without including the position-dependent correction term. Let us first investigate the depen-

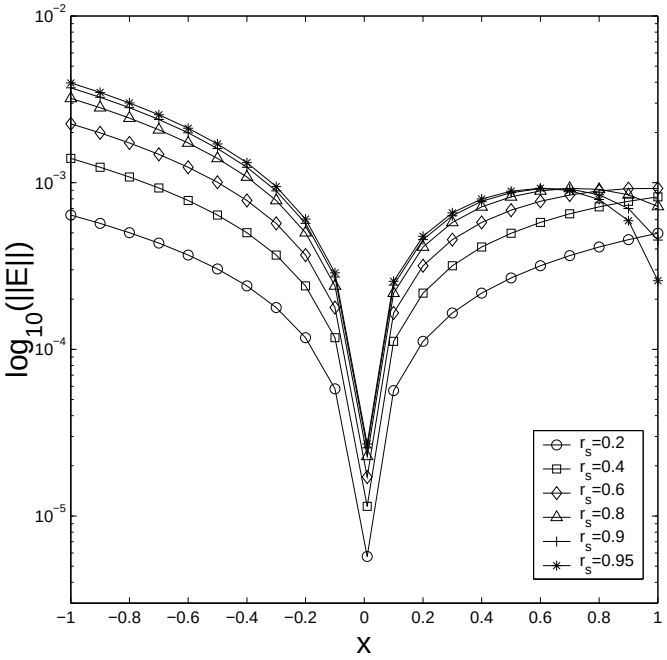

Figure 2: The relative errors of the second-order image approximation in the reaction field at 21 observation points equally spaced on the x-axis, from -1 to 1, for six different source locations.

dence of the accuracy of the second-order image approximation on the source location. To this end, in this test the inverse Debye screening length is set as $\lambda = 0.5$, and the Jacobi-Gauss-Radau quadrature with $M = 20$ is employed to approximate the underlying line image. For each selected source position, we calculate the relative error of the image approximation in the reaction field, respectively, at 21 observation points equally spaced on the x-axis, from -1 to 1. The results are displayed in Fig. 2. As can be seen, the approximation error increases as the source moves to the spherical boundary while the observation point is fixed, or similarly as the observation point moves to the spherical boundary while the source is fixed. In addition, for all cases where $r_s < 0.95$, the relative error in the reaction potential is less than 10^{-2}. It should be noted that, for the cases where $r_s \geq 0.9$, using only 400 terms in the series expansion could be insufficient for us to calculate accurate enough "exact reaction fields" at those observation points close to the spherical boundary. And it is believed to be the reason why the error plots corresponding to the cases where $r_s \geq 0.9$ exhibit some abnormal behaviors at those points near the spherical boundary.

5.3 Direct series expansion vs image approximation

In the case that the point charge is close to the spherical boundary, the Kelvin image point $\mathbf{r}_i$ is also close to the boundary. Therefore, when calculating the reaction field at a point

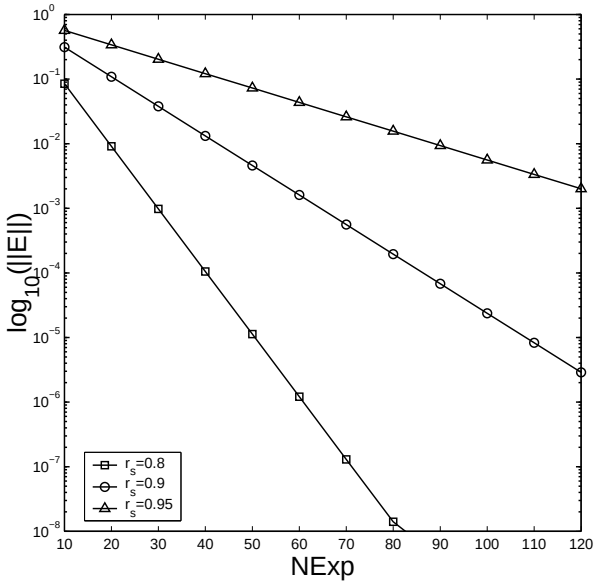

Figure 3: The maximal relative errors of the method of direct series expansion in the reaction field at 21 observation points equally spaced on the x-axis, from -1 to 1, for three different source locations, where $NExp$ represents the number of terms included in the direct series expansion.

close to the spherical boundary, the convergence by the direct series expansion

$$\Phi_{\rm RF}(r,\theta)=\sum_{n=0}^{\infty}A_n r^n P_n(\cos\theta)=\frac{q}{4\pi\epsilon_{\rm i}a}\sum_{n=0}^{\infty}\frac{\epsilon_{\rm i}(n+1)k_n(u)+\epsilon_{\rm o}uk_n'(u)}{\epsilon_{\rm i}nk_n(u)-\epsilon_{\rm o}uk_n'(u)}\left(\frac{r}{r_{\rm i}}\right)^n P_n(\cos\theta)$$

will be slow due to $r/r_{\rm i}\approx 1$, requiring a great number of terms to achieve high accuracy in the reaction field.

To compare the method of direct series expansion and the second-order image approximation, in this test the inverse Debye screening length is again fixed at $\lambda=0.5$, while the Jacobi-Gauss-Radau quadrature with $M=2$ is used to discretize the line image. Three different source locations with $r_{\rm s}=0.8$, 0.9 and 0.95 are tested, respectively. For each selected source location, we approximate the reaction fields at the same 21 points on the x-axis by the direct series expansion with various numbers of terms, compare the results to the exact ones obtained by the direct series expansion with 400 terms, calculate and plot in Fig. 3 the maximal relative errors. As indicated in Fig. 3, more than 20, 40 and 80 terms have to be included for the approximation error to be less than 10^{-2} for the cases of $r_{\rm s}=0.8$, 0.9 and 0.95, respectively. On the other hand, the corresponding errors of the second-order image approximation with $M=2$ are 3.07×10^{-3}, 3.53×10^{-3}, and 3.76×10^{-3}, respectively, all less than 10^{-2} already! Therefore, to calculate reaction fields at points close to the spherical boundary due to point charges also close to the boundary, the second-order image approximation is clearly much more efficient than the method of direct series expansion.

Table 2: Relative errors of the second-order image approximation using different numbers of point images.

	$r_s=0.5$				$r_s=0.95$			
$u=\lambda a$	$M=0$	$M=1$	$M=2$	$M=20$	$M=0$	$M=1$	$M=2$	$M=20$
0.8	2.57E-2	3.41E-3	3.45E-3	3.45E-3	2.58E-2	7.16E-3	7.37E-3	7.37E-3
0.4	2.80E-2	1.25E-3	1.29E-3	1.29E-3	3.01E-2	3.52E-3	2.85E-3	2.85E-3
0.2	2.90E-2	3.64E-4	4.03E-4	4.01E-4	3.21E-2	3.65E-3	1.01E-3	9.00E-4
0.1	2.94E-2	1.25E-4	1.14E-4	1.12E-4	3.29E-2	3.69E-3	1.04E-3	2.54E-4
0.05	2.98E-2	1.63E-4	3.13E-5	2.97E-5	3.31E-2	3.70E-3	1.05E-3	6.76E-5
0.025	2.96E-2	1.73E-4	9.21E-6	7.65E-6	3.32E-2	3.70E-3	1.06E-3	1.74E-5
0.0125	2.96E-2	1.75E-4	3.76E-6	1.94E-6	3.33E-2	3.70E-3	1.06E-3	4.43E-6

5.4 Accuracy vs the number of discrete point images

One natural concern with the proposed second-order image approximation is the final number of discrete point images required to achieve a certain order of degree of accuracy. For a desired accuracy, this number depends on the locations of both the source charge and the observation point. It should be small if compared to the number of terms needed to achieve the same degree of accuracy in the direct series expansion to make the image approximations useful in the practice.

It has been observed that for relatively large values of $u=\lambda a$, two to three images including the point image at the Kelvin image point ($M=1$ or 2) are sufficient for the second-order image approximation to achieve the best possible results, and using more images will not further improve the overall accuracy of the scheme. This can be understood by the fact that the overall accuracy of the scheme is determined by the combined effect of the error arising in the approximation of the reaction field by a line image and that arising in the discretization of the line image by discrete point images. Although in principle, the latter can be reduced to zero (limited only by machine precision) by using a sufficient number of point images, the former is irreducible for a fixed ionic strength, suggesting that by no means the accuracy of the scheme can exceed that of the line image approximation. For example, as indicated in Table 2, for the case of $r_s=0.95$ and $u=0.8$, the error of the line image approximation is around 7.37×10^{-3}. Therefore, no matter how many point images are used to discretize the line image, the best possible accuracy of the overall scheme shall be limited by this error.

For relatively small values of $u=\lambda a$, the error of the line image approximation is small. In this case, in order to realize the best possible result, more discrete point images have to be introduced so that the approximation error from the discretization of the involved line image is smaller. For example, for the case of $r_s=0.95$ and $u=0.1$, the best possible accuracy of the scheme appears to be around 2.54×10^{-4}, but using three discrete point images can only achieve an accuracy of 1.04×10^{-3}. For the overall accuracy of the image method to be less than 10^{-2}, however, still only two to three images including the point image at the Kelvin image point ($M=1$ or 2) are needed.

6 Conclusions

In this paper, we have presented two discrete image approximations to the reaction field due to a point charge inside a dielectric sphere of radius a immersed in an ionic solvent for small values of $u = \lambda a$ (λ – the inverse Debye screening length of the ionic solvent, a – the radius of the dielectric sphere). A first-order image approximation is first obtained using a point image at the Kelvin image point and a line image that extends from the Kelvin image point out to infinity. Then, this first-order image approximation is improved by including one or two correction potentials, resulting in a second-order image approximation. The line image is further approximated by an equivalent set of discrete images. Numerical results have demonstrated that only two to three point images are needed for the second-order image approximation to achieve a 10^{-3} accuracy in the reaction field. Studies of high-order image approximations are in progress and will be reported in a forthcoming paper.

Applications of the proposed second-order image approximation for calculating the electrostatic force interactions in protein folding and materials under extreme conditions such as strong irradiations are in progress. As a final remark, using the fast multipole methods [19,20], the second-order image method presented in this paper has the potential to result in an $\mathcal{O}(N)$ algorithm [13] for calculating electrostatic interactions for N atoms in a dielectric sphere immersed in an ionic solvent.

Acknowledgments

The authors thank the support of the National Science Foundation (grant numbers: DMS-0408309, CCF-0513179), the Department of Energy (grant number: DEFG0205ER25678), and the NERSC Computing Award for the work reported in this paper. The authors also thank Drs. Andriy Baumketner and Donald Jacobs for many interesting discussions.

References

[1] P. Koehl, Electrostatics calculations: latest methodological advances, Curr. Opin. Struc. Biol., 16 (2006), 142-151.
[2] R. M. Levy and E. Gallicchio, Computer simulations with explicit solvent: recent progress in the thermodynamic decomposition of free energies and in modeling electrostatic effects, Annu. Rev. Phys. Chem., 49 (1998), 531-567.
[3] C. Sagui and T. A. Darden, Molecular dynamics simulation of biomolecules: Long-range electrostatic effects, Annu. Rev. Biophys. Biomol. Struc., 28 (1999), 155-179.
[4] M. Feig and C. L. Brooks III, Recent advances in the development and application of implicit solvent models in biomolecule simulations, Curr. Opin. Struc. Biol., 14 (2004), 217-224.
[5] N. A. Baker, Improving implicit solvent simulations: A Poisson-centric view, Curr. Opin. Struc. Biol., 15 (2005), 137-143.
[6] A. Okur and C. Simmerling, Hybrid explicit/implicit solvation methods, in: D. Spellmeyer (Ed.), Annu. Rep. Comput. Chem., Vol. 2, 2006, Chapter 6.

[7] M. S. Lee, F. R. Salsbury JR. and M. A. Olson, An efficient hybrid explicit/implicit solvent method for biomolecular simulations, J. Comput. Chem., 25 (2004), 1967-1978.
[8] M. S. Lee and M. A. Olson, Evaluation of Poisson solvation models using a hybrid explicit/implicit solvent method, J. Phys. Chem. B, 109 (2005), 5223-5236.
[9] C. L. Brooks and M. Karplus, Deformable stochastic boundaries in molecular-dynamics, J. Chem. Phys., 79 (1983), 6312-6325.
[10] C. L. Brooks, A. Brunger and M. Karplus, Active-site dynamics in protein molecules - a stochastic boundary molecular-dynamics approach, Biopolymers, 24 (1985), 843-865.
[11] G. King and A. Warshel, A surface constrained all-atom solvent model for effective simulations of polar solutions, J. Chem. Phys., 91 (1989), 3647-3661.
[12] D. Belgov and B. Roux, Finite representation of an infinite bulk system - Solvent boundary potential for computer simulations, J. Chem. Phys., 100 (1994), 9050-9063.
[13] W. Cai, S. Deng and D. Jacobs, Extending the fast multipole method to charges inside or outside a dielectric sphere, J. Comput. Phys., 223 (2007), 846-864.
[14] J. G. Kirkwood, Theory of solutions of molecules containing widely separated charges with special applications to awitterions, J. Chem. Phys., 2 (1934), 351-461.
[15] J. G. Kirkwood, Statistical mechanics of liquid solutions, Chem. Rev., 19 (1936), 275-307.
[16] I. G. Tironi, R. Sperb, P. E. Smith and W. F. van Gunsteren, A generalized reaction field method for molecular dynamics simulation, J. Chem. Phys., 102 (1995), 5451-5459.
[17] C. Tanford and J. G. Kirkwood, Theory of protein titration curves. I. General equations for impenetrable spheres, J. Am. Chem. Soc., 79 (1957), 5333-5339.
[18] J. A. Barker, Reaction field, screening, and long-range interactions in simulations of ionic and dipolar systems, Mol. Phys., 83 (1994), 1057-1064.
[19] L. Greengard and V. Rokhlin, A fast algorithm for particle simulations, J. Comput. Phys., 73 (1987), 325-348.
[20] L. Greengard, The Rapid Evaluation of Potential Fields in Particle Systems, MIT, Cambridge, 1987.
[21] H. L. Friedman, Image approximation to the reaction field, Mol. Phys., 29 (1975), 1533-1543.
[22] R. Abagyan and M. Totrov, Biased probability Monte Carlo conformational searches and electrostatic calculations for peptides and proteins, J. Mol. Biol., 235 (1994), 983-1002.
[23] A. Wallqvist, On the implementation of Friedman boundary conditions in liquid water simulations, Mol. Simul., 10 (1993), 13-17.
[24] L. Wang and J. Hermans, Reaction field molecular dynamics simulation with Friedman's image method, J. Phys. Chem., 99 (1995), 12001-12007.
[25] J. A. C. Rullmann and P. Th. V. Duijnen, Analysis of discrete and continuum dielectric models: application to the calculation of protonation energies in solution, Mol. Phys., 61 (1987), 293-311.
[26] G. Petraglio, Nonperiodic boundary conditions for solvated systems, J. Chem. Phys., 123 (2005), 044103.
[27] J. J. Havranek and P. B. Harbury, Tanford-Kirkwood electrostatics for protein modeling, Proc. Nat. Acad. Sci. USA, 96 (1999), 11145-11150.
[28] C. Neumann, Hydrodynamische Untersuchen nebst einem Anhang uber die Probleme der Elecktrostatik und der magnetischen Induktion, Teubner, Leipzig, 1883, 279-282.
[29] J. D. Jackson, Classical Electrodynamics, John Wiley, New York, 1999.
[30] I. V. Lindell, Electrostatic image theory for the dielectric sphere, Radio Sci., 27 (1992), 1-8.
[31] I. V. Lindell, M. E. Ermutlu and A. H. Sihvola, Electrostatic image theory for layered dielectric sphere, IEE Proc. H, 139 (1992), 186-192.

[32] I. V. Lindell, Image theory for electrostatic and magnetostatic problems involving a material sphere, Am. J. Phys., 61 (1993), 39-44.
[33] W. T. Norris, Charge images in a dielectric sphere, IEE Proc.-Sci. Meas. Tech., 142 (1995), 142-150.
[34] J. Warwicker and H. C. Watson, Calculation of the electric potential in the active site cleft due to alpha-helix dipoles, J. Mol. Biol., 157 (1982), 671-679.
[35] N. A. Baker, Poisson-Boltzmann methods for biomolecular electrostatics, Method. Enzymol., 383 (2004), 94-118.
[36] F. Fogolari, A. Brigo and H. Molinari, The Poisson-Boltzmann equation for biomolecular electrostatics, J. Mol. Biol., 15 (2002), 377-392.
[37] A. J. Bordner and G. A. Huber, Boundary element solution of the linear Poisson-Boltzmann equation and a multipole method for the rapid calculation of forces on macromolecules in solution, J. Comput. Chem., 24 (2003), 353-367.
[38] A. Juffer, E. F. F. Botta, B. A. M. van Keulen, A. van der Ploeg and H. J. C. Berendsen, The electric potential of a macromolecule in a solvent: A fundamental approach, J. Comput. Phys., 97 (1991), 144-171.
[39] H. Alper and R. M. Levy, Dielectric and thermodynamic response of a generalized reaction field model for liquid state simulations, J. Chem. Phys., 99 (1993), 9847-9852.
[40] P. M. Morse and H. Feshbach, Methods of Theoretical Physics, McGraw-Hill, New York, 1953.
[41] L. F. Greengard and J. Huang, A new version of the fast multipole method for screened Coulomb interactions in three dimensions, J. Comput. Phys., 180 (2002), 642-658.
[42] M. Abramowitz and I. A. Stegun, Handbook of Mathematical Functions with Formulas, Graphs, and Mathematical Tables, Dover Publications, New York, 1972.
[43] I. S. Gradshteyn and I. M. Ayzhik, Table of Integrals, Series, and Products, Academic Press, Boston, 1994.
[44] W. Gautschi, Algorithm 726; ORTHPOL - a package of routines for generating orthogonal polynomials and Gauss-type quadrature rules, ACM T. Math. Software, 20 (1994), 21-62.